Current Optics and Photonics
Vol. 3, No. 3, June 2019, pp. 236-242

ISSN: 2508-7266(Print) / ISSN: 2508-7274(Online)
DOI: https://doi.org/10.3807/COPP.2019.3.3.236

Design of an Nd:YAG Slab Structure for a High-power Zigzag Slab Laser Amplifier Based on a Wavefront Simulation

Jae Sung Shin*, Yong-Ho Cha, and Byung Heon Cha

Korea Atomic Energy Research Institute, Daejeon 34057, Korea

(Received January 14, 2019 : revised April 12, 2019 : accepted April 16, 2019)

An Nd:YAG slab structure was designed for a high-power zigzag slab laser amplifier based on computational simulation of the wavefront distortion. For the simulation, the temperature distribution in the slab was calculated at first by thermal analysis. Then, the optical path length (OPL) was obtained by a ray tracing method for the corresponding refractive index variation inside the slab. After that, the OPL distribution of the double-pass amplified beam was calculated by summing the results obtained for the first and second passes. The amount of wavefront distortion was finally obtained as the peak-to-valley value of the OPL distribution. As a result of this study, the length and position of the gain medium were optimized by minimizing the transverse wavefront distortion. Under the optimized conditions, the transverse wavefront distortion of the double-pass amplified beam was less than 0.2 μm for pump power of 14 kW.

Keywords : Zigzag slab laser, High-power laser, Laser amplifier, Wavefront distortion
OCIS codes : (140.3280) Laser amplifiers; (140.3460) Lasers; (140.3530) Lasers, neodymium; (140.3580) Lasers, solid-state

I. INTRODUCTION

Zigzag slab geometry has been used to achieve high-quality beams in high-average-power solid-state lasers [1-12]. In the zigzag slab structure, the seed beam is amplified by bouncing from the inside of the gain medium several times by total internal reflection. This zigzag propagation improves the beam quality in the transverse direction by averaging out the wavefront distortion generated from the thermal gradient in the slab [1]. On the other hand, since the beam propagates straight ahead inside the slab for the vertical direction rather than zigzag, the vertical wavefront distortion can be large depending on the pump beam profile, the optical design of the pump light delivering components, the cooling uniformity, and so on. Therefore, in previous studies, techniques for minimizing vertical wavefront distortion have mainly focused on improving the beam quality [10-12]. The occurrence of transverse wavefront distortion has not been considered much in the design of laser amplifiers.

However, despite the zigzag propagation, wavefront distortion for the transverse direction also occurs in the zigzag slab laser. The amount of transverse wavefront distortion is small, but it can be a problem if the seed beam is amplified by multiple chains for a high-power laser output. Considering that the wavelength of a zigzag slab laser is typically 1 μm, a small amount of 1 μm distortion acts as a phase fluctuation of 2π. Therefore, it is also important to reduce the transverse wavefront distortion as well as the vertical distortion.

Our previous study showed that the amount of transverse wavefront distortion is related to the length of the gain medium [11]. If the length of the gain medium is an integer multiple of half of the zigzag period, the transverse wavefront distortion can be minimized. This is because the total optical path lengths for all points in the transverse direction are nearly the same under these conditions, as the ray of each point passes almost the same distance alternating between the cold edge and the hot center. Therefore, in the case of single-pass amplification with a

*Corresponding author: jsshin12@kaeri.re.kr, ORCID 0000-0001-6245-1710
Color versions of one or more of the figures in this paper are available online.

certain incident angle, the transverse wavefront distortion can be minimized by determining the length of the gain medium accordingly. However, double-pass amplification is applied more than single-pass amplification in high-power operation. In this case, zigzag slab lasers generally have an amplification structure in which the first pass and the second pass have different incident angles. Thus, if the length of the gain medium is determined by considering only one incident angle, the transverse wavefront distortion may be large for the other incident angle. For this reason, the slab structure should be determined considering both angles.

In this work, an Nd:YAG slab structure was designed for double-pass amplification in a high-power zigzag slab laser amplifier. For this purpose, the transverse wavefront distortion was computationally simulated considering the zigzag propagation with two different incident angles. The length and position of the gain medium were optimized by minimizing the transverse wavefront distortion.

II. SIMULATION CONDITIONS AND PROCEDURE

Figure 1 shows the conceptual scheme of the double pass amplification of the Nd:YAG slab, which was used for design of the slab structure. In this structure, pure YAGs are located at both ends of the Nd:YAG. The slab entrance and exit are cut at 45 degrees. The total length of the slab is denoted by L_s, and the length of the Nd:YAG is denoted by L_d. The position of the Nd:YAG is denoted by X_d, which means the distance from the left end of the slab to the right end of the Nd:YAG.

Generally, in the case of a double pass amplification to obtain a high power beam in a zigzag slab laser, the slab incident angles are made slightly different from each other to make a difference in path between the first and the second amplifications. This is because the depolarized beam can be returned to the opposite direction in the case of a scheme of amplifying the same path twice by using a change in polarization. The difference in amplification path also allows for more extraction of the stored energy in the gain medium. Thus, this scheme was used for the simulation. The incident angle of the first amplification pass is denoted by θ_1, and that of the second amplification pass is denoted by θ_2.

In the simulation, an end-pumped scheme was assumed, which was symmetrically pumped for both ends. Ideally uniform pumping in the height direction of the slab was considered since only the transverse wavefront distortion was of interest. The slab was 30 mm high, 2.5 mm wide, and 120 mm long (L_s). The incident angles, θ_1 and θ_2, were determined so that the entire beam meets the condition of total internal reflection inside the slab. Here, θ_1 was set to be 22 degrees which means that the beam is bounded 30 times inside the slab, and θ_2 was set to be 18.5 degrees which means that the beam is bounced 28 times inside the slab. The doping concentration of the Nd:YAG was 0.2 at.%. Both sides of the slab were assumed to be uniformly cooled to a temperature of 293 K with a film coefficient of 0.33 W/mm^2 · K, and the width of the incident seed beam was set to be 3 mm.

The simulation of the wavefront distortion proceeded in the following order. The detailed simulation methodology is well described in our previously reported papers [10, 11] and is omitted in this paper. First, the temperature distribution in the slab was calculated by thermal analysis. Then, the obtained temperature distribution was used to calculate the refractive index variation inside the slab. Thereafter, the optical path length (OPL) was calculated with the ray tracing method for each ray constituting the laser beam after passing through the slab. After that, the OPL distribution of the double-pass amplified beam was calculated by summing the results obtained for the first and second passes. The amount of wavefront distortion was finally obtained as the peak-to-valley value of the OPL distribution. Based on the simulation results, the slab structure was optimized to minimize the transverse wavefront distortion.

III. RESULTS AND DISCUSSION

3.1. Temperature Distribution

Figure 2 shows the temperature distributions of the slab for the total pump power of 14 kW, which can extract the laser power of ~4.5 kW. Figure 2(a) shows the temperature distribution for the slab length axis at the center of the width, and Fig. 2(b) shows the temperature distribution for

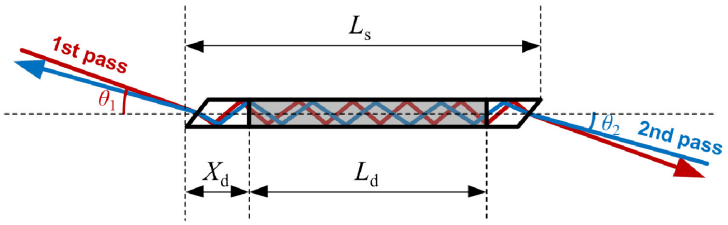

FIG. 1. Conceptual scheme of the Nd:YAG zigzag slab amplifier for design optimization (L_s: total length of the slab, L_d: length of the Nd:YAG, X_d: distance from the left end of the slab to the right end of the Nd:YAG, θ_1: incident angle of the first amplification pass, θ_2: incident angle of the second amplification pass).

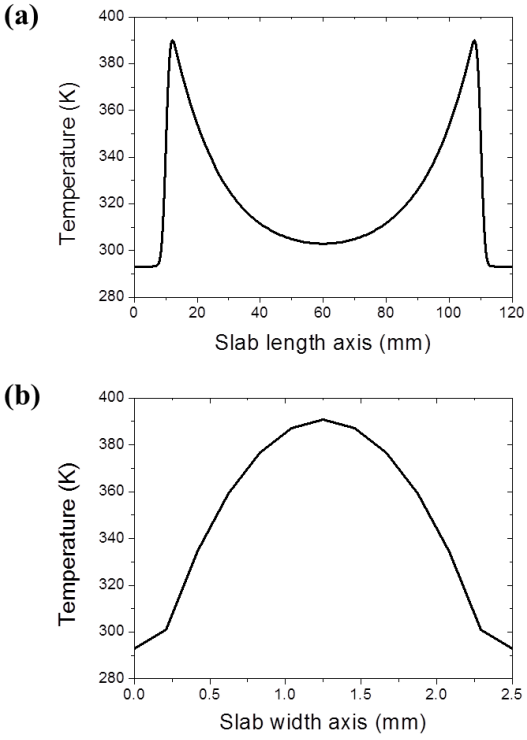

FIG. 2. Temperature distributions (a) for slab length axis at the center of the width and (b) for slab width axis at the temperature peak position of the length when the total pump power was 14 kW. Here, L_d and X_d are 100 mm and 10 mm, respectively, so that the lengths of the pure YAGs located at both ends would be equal.

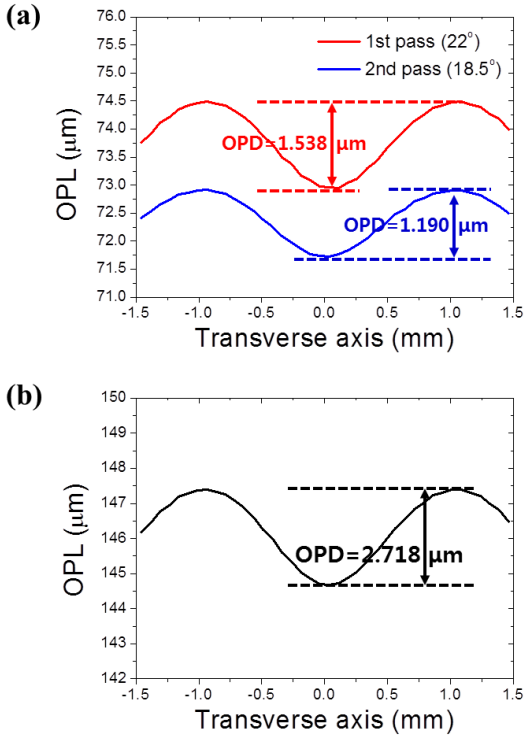

FIG. 3. OPL distributions for transverse axis of the amplified beam when L_d and X_d were 100 mm and 10 mm, respectively: (a) OPL distributions for the first pass ($\theta_1 = 22°$) and for the second pass ($\theta_2 = 18.5°$), (b) OPL distribution for the double pass.

the slab width axis at the temperature peak position of the length. In this case, L_d and X_d were set to be 100 mm and 10 mm, respectively, so that the lengths of the pure YAGs located at both ends would be equal.

As seen in the temperature distribution for the length axis direction shown in Fig. 2(a), the temperature rapidly increased from the interface between the pure YAG and the Nd:YAG, since the pump beam started to be absorbed at the front surface of the Nd:YAG. The temperature showed a peak after a few millimeters (~2 mm) from the interface boundary, and the peak value was 390 K. As seen in the temperature distribution for the width axis direction at this position, the center of the slab width had the highest temperature and lower temperatures toward the side. The temperatures of the side edges were 293 K because the slab was cooled to this temperature.

In the other conditions of L_d and X_d, the shape of the temperature distribution was similar to that of Fig. 2, except that the position of the peak shifted slightly due to the interface position change of the pure YAG and the Nd:YAG. Thus, these results have been omitted from this paper.

3.2. Determination of the Nd:YAG Length

As mentioned before, the refractive index variation inside the slab was calculated from the obtained temperature distribution. From the result of the refractive index variation, the OPL distribution could be obtained by the ray tracing method. Figure 3 shows the OPL distributions for the transverse axis of the amplified beam when L_d and X_d were 100 mm and 10 mm, respectively. Figure 3(a) shows the OPL distributions for the first pass ($\theta_1 = 22°$) and for the second pass ($\theta_2 = 18.5°$). Figure 3(b) shows the OPL distribution after the double pass amplification. The optical path differences (OPDs), which mean the peak-to-valley values of the OPLs, were 1.538 μm for the first pass and 1.190 μm for the second pass. The OPL values of the first pass were larger than those of the second pass because the first pass with larger incident angle bounds more inside the slab than the second pass. In this case, the OPDs for the double pass, which are obtained from the sum of the OPL values for the first and the second passes, is 2.718 μm.

Similarly, the OPDs with respect to the Nd:YAG length (L_d) were calculated near $L_d = 100$ mm. At this time, the values of X_d were determined to satisfy $X_d = (L_s - L_d)/2$ so that the Nd:YAG was positioned at the center of the total slab length. Figure 4 shows the OPDs for the transverse axis with respect to L_d. Figure 4(a) shows the OPDs for the first pass ($\theta_1 = 22°$) and for the second pass ($\theta_2 = 18.5°$). Figure 4(d) shows the OPDs for the double pass.

As shown in Fig. 4(a), the OPDs for the single pass periodically changed with respect to L_d. In this case, the

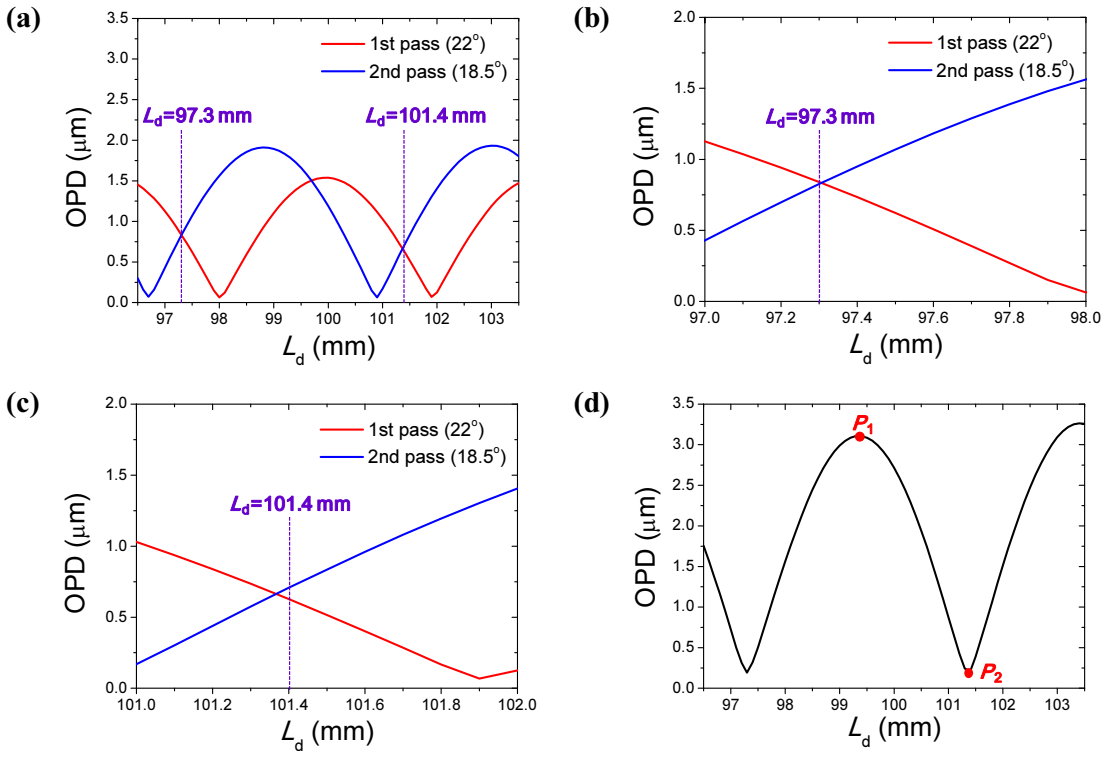

FIG. 4. OPDs with respect to the Nd:YAG length (L_d) for transverse axis of the amplified beam when the values of X_d were determined to satisfy $X_d = (L_s - L_d)/2$ so that the Nd:YAG was positioned at the center of the total slab length: (a) OPDs for the first pass ($\theta_1 = 22°$) and for the second pass ($\theta_2 = 18.5°$), (b) rescaled OPDs near $L_d = 97.3$ mm, (c) rescaled OPDs near $L_d = 104.4$ mm, (d) OPDs for the double pass.

period of the OPD variation was half of the zigzag period. Geometrically, the zigzag period (T) can be easily calculated by Snell's law as

$$T = \frac{2w}{\tan\left[45° - \sin^{-1}\left[\frac{1}{n}\sin(45° - \theta)\right]\right]}, \quad (1)$$

where w is the width of the slab (= 2.5 mm), n is the refractive index of YAG (= 1.82), and θ is the incident angle for each pass. The zigzag period for the first pass (T_1) was 7.82 mm, and the corresponding period of the OPD variation was 3.91 mm. The zigzag period for the second pass (T_2) was 8.38 mm, and the corresponding period of the OPD variation was 4.19 mm. Thus, the neighboring local minima of OPDs were 3.91 mm apart for the first pass and 4.19 mm apart for the second pass.

As shown in Fig. 4(d), the OPDs for the double pass also varied periodically. The OPDs for the double pass depended on the amount of the OPDs for each pass and the phase relation of the OPL distributions between the first and the second passes. Figure 5 shows the OPL distributions for two cases with the OPDs at a local maximum point (P_1) where $L_d = 97.3$ mm and at a local minimum point (P_2) where $L_d = 101.4$ mm. Figure 5(a) shows the OPL distributions at P_1 for the first pass ($\theta_1 = 22°$) and for the second pass ($\theta_2 = 18.5°$), and Fig. 5(b) shows the OPL distribution at P_1 for the double pass. Figure 5(c) shows the OPL distributions at P_2 for the first pass ($\theta_1 = 22°$) and for the second pass ($\theta_2 = 18.5°$), and Fig. 5(d) shows the OPL distribution at P_2 for the double pass. At the local maximum P_1, as shown in Fig. 5(a), the OPDs of the first and second passes are moderately large, and the OPL distributions are in phase with each other. At the local minimum P_2, as shown in Fig. 5(c), the OPDs of the first and the second passes are small and almost equal, and the OPL distributions are out of phase with each other.

As a result, the OPDs for the double pass are minimized if the magnitudes of the OPDs of the first and the second passes are equal and the OPL distributions are out of phase with each other. Thus, the Nd:YAG length can be determined so that the OPDs of the first and the second passes are nearly equal to each other. When considering 0.1 mm spacing, the Nd:YAG lengths meet these conditions near 100 mm are $L_d = 97.3$ mm and $L_d = 101.4$ mm, as shown in Fig. 4(a). Figures 4(b) and 4(c) show rescaled OPDs at these points, showing that the OPDs of the first and the second passes are almost equal to each other. For these Nd:YAG lengths, the transverse wavefront distortion can be minimized only if the conditions in which the OPL distributions of the first and the second passes are out of phase are satisfied.

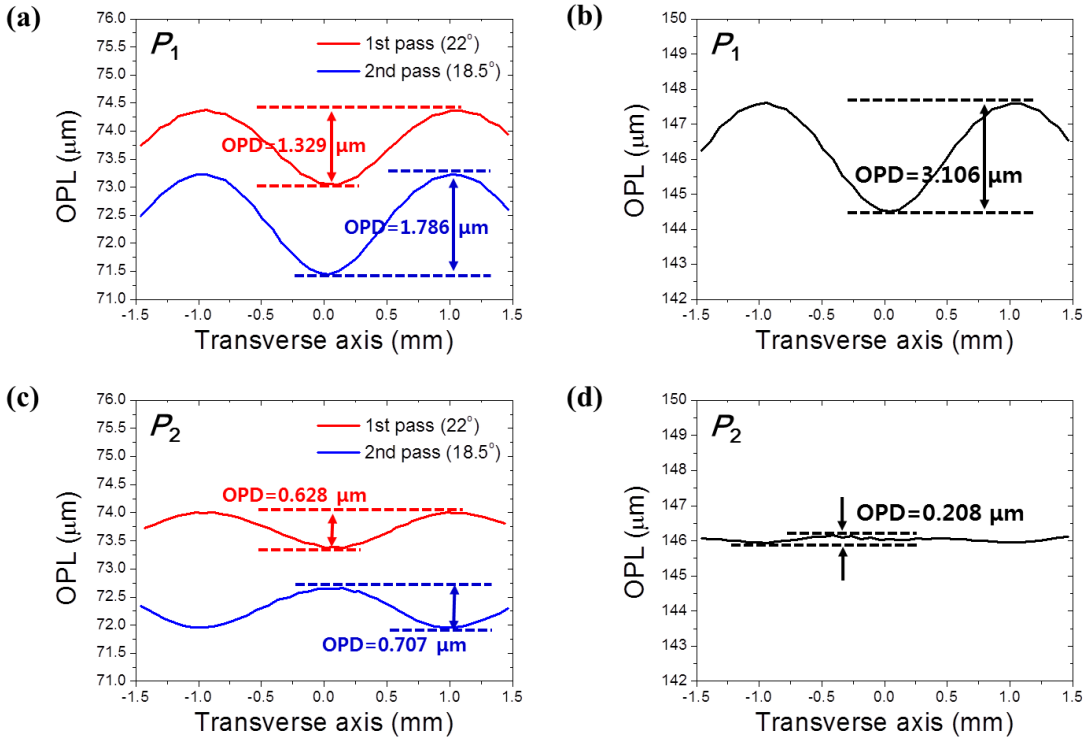

FIG. 5. OPL distributions for transverse axis of the amplified beam at a local maximum point (P_1) where L_d = 97.3 mm and at a local minimum point (P_2) where L_d = 101.4 mm: (a) OPL distributions for the first pass ($\theta_1 = 22°$) and for the second pass ($\theta_2 = 18.5°$) at P_1, (b) OPL distribution for the double pass at P_1, (c) OPL distributions for the first pass ($\theta_1 = 22°$) and for the second pass ($\theta_2 = 18.5°$) at P_2, OPL distribution for the double pass at P_2.

3.3. Determination of the Nd:YAG Position

In the previous section, two candidates for the Nd:YAG length were determined. One is for $L_d = 97.3$ mm and the other is for and $L_d = 101.4$ mm. As mentioned in Section 3.2, the OPL distributions for the first and the second passes should be out of phase to minimize the transverse wavefront distortion. Because the phase of the OPL distribution depends on the position of the Nd:YAG, the OPDs were evaluated by varying the Nd:YAG position (X_d) for the two Nd:YAG length candidates.

Figures 6(a) and 6(b) show the OPDs for each pass and for the double pass, respectively, when $L_d = 97.3$ mm. Figures 6(c) and 6(d) show the corresponding OPD results when $L_d = 101.4$ mm. In both cases, if L_d is constant, the OPDs of the first and second passes are almost constant even though X_d varies. Therefore, the variation of X_d is almost related only to the phase change of the OPL distribution. As shown in Fig. 6(b) when $L_d = 97.3$ mm, the local minima were located at X_d of 7.3 mm, 9.3 mm and 11.3 mm. Thus, the transverse wavefront could be minimized at these positions of Nd:YAG. For these cases, the OPL distributions for the first and second passes were out of phase, and the OPDs were 0.199 μm, 0.164 μm, and 0.166 μm for X_d of 7.3 mm, 9.3 mm and 11.3 mm, respectively. Similarly, as shown in Fig. 6(d), when L_d = 101.4 mm, the local minima were located at X_d of 7.2 mm, 9.3 mm, and 11.3 mm. Since the length difference between 97.3 mm and 101.4 mm was small, the positions of local minima for the two different lengths were almost the same. In the case of $L_d = 101.4$ mm, the OPDs were 0.188 μm, 0.208 μm, and 0.164 μm for X_d of 7.2 mm, 9.3 mm, and 11.3 mm, respectively.

Figure 7 shows the OPL distributions for two cases with the OPD values at a local maximum point (P_3) where $X_d = 9.3$ mm and at a local minimum point (P_4) where $X_d = 10.3$ mm. Figure 7(a) shows the OPL distributions at P_3 for the first pass ($\theta_1 = 22°$) and for the second pass ($\theta_2 = 18.5°$), and Fig. 7(b) shows the OPL distribution at P_3 for the double pass. At the local maximum P_3, as shown in Fig. 7(b), the OPL distributions for the first and second passes were in phase with each other. In this case, the OPD for the double pass was 1.641 μm. Figure 7(c) shows the OPL distributions at P_4 for the first pass (θ_1 = 22°) and for the second pass ($\theta_2 = 18.5°$), and Fig. 7(d) shows the OPL distribution at P_4 for the double pass. At the local minimum P_4, as shown in Fig. 7(c), the OPL distributions for the first and second passes were out of phase with each other. In this case, the OPD for the double pass was 0.164 μm.

As a result, the transverse wavefront distortion was minimized for the cases of $X_d = 7.3$ mm, 9.3 mm, and 11.3 mm when $L_d = 97.3$ mm and $X_d = 7.2$ mm, and 9.3 mm and 11.3 mm when $L_d = 101.4$ mm. Any designs can be selected for the Nd:YAG structure in a zigzag slab laser amplifier.

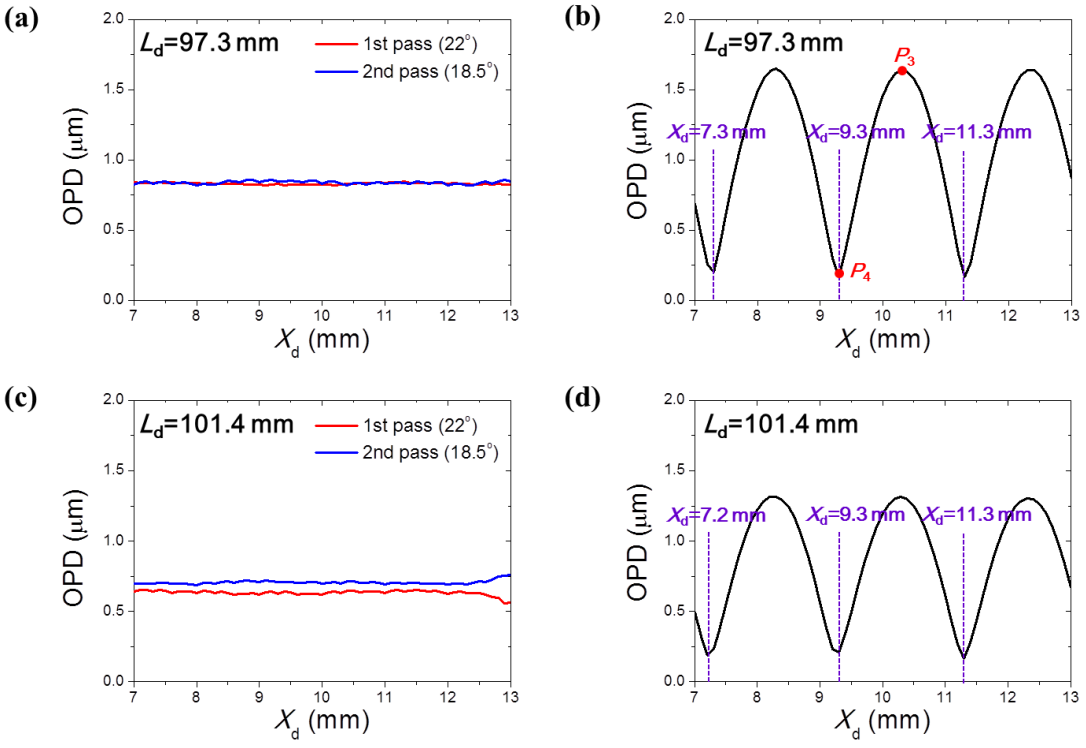

FIG. 6. OPDs with respect to the Nd:YAG position (X_d) for transverse axis of the amplified beam: (a) OPDs for the first pass (θ_1 = 22°) and for the second pass (θ_2 = 18.5°) when L_d = 97.3 mm, (b) OPDs for the double pass when L_d = 97.3 mm, (c) OPD values for the first pass (θ_1 = 22°) and for the second pass (θ_2 = 18.5°) when L_d = 101.4 mm, (d) OPD values for the double pass when L_d = 101.4 mm.

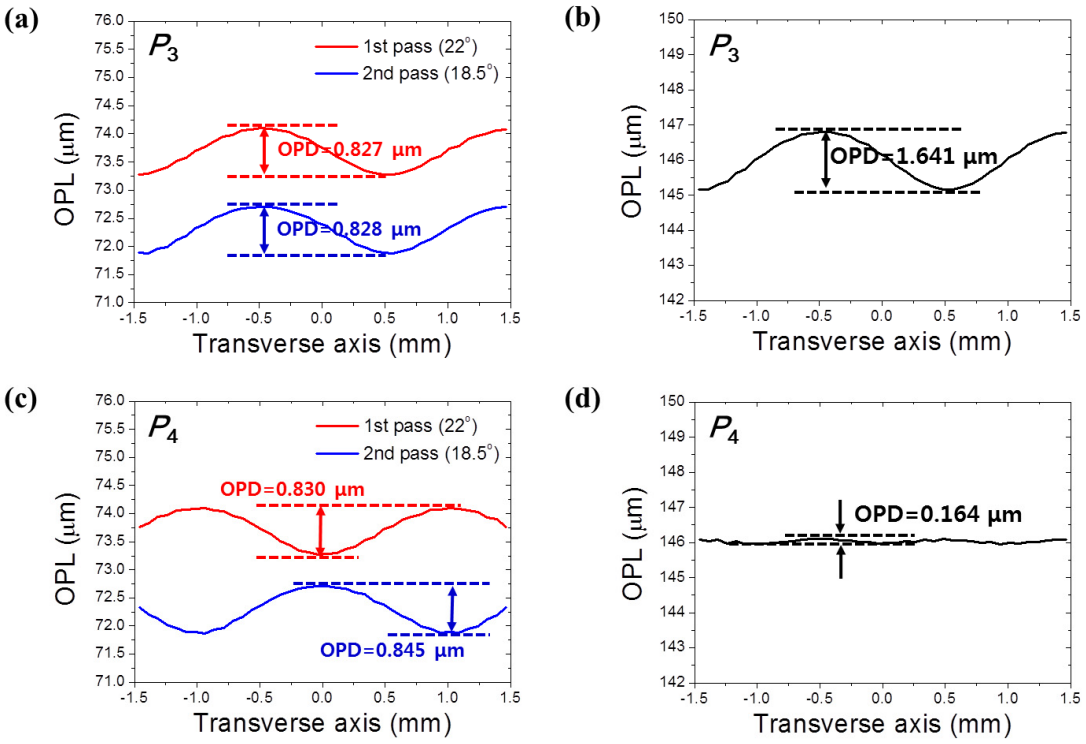

FIG. 7. OPL distributions for transverse axis of the amplified beam when L_d = 97.3 mm at a local maximum point (P_3) where X_d = 10.3 mm and at a local minimum point (P_4) where X_d = 9.3 mm: (a) OPL distributions for the first pass (θ_1 = 22°) and for the second pass (θ_2 = 18.5°) at P_3, (b) OPL distribution for the double pass at P_3, (c) OPL distributions for the first pass (θ_1 = 22°) and for the second pass (θ_2 = 18.5°) at P_4, OPL distribution for the double pass at P_4.

IV. CONCLUSION

In summary, an Nd:YAG slab structure was designed for a high-power zigzag slab laser amplifier. For this purpose, computational simulations were performed to calculate the transverse wavefront distortion considering double-pass amplification with two different incident angles. Based on the simulation results, the length and position of the gain medium were optimized by minimizing the transverse wavefront distortion. As a result, the transverse wavefront distortion could be minimized for the cases that the position of the Nd:YAG (X_d) was 7.3 mm, 9.3 mm, or 11.3 mm when the length of the Nd:YAG (L_d) is 97.3 mm. The transverse wavefront distortion could be also minimized when the position of the Nd:YAG (X_d) was 7.2 mm, 9.3 mm, or 11.3 mm and the length of the Nd:YAG (L_d) was 101.4 mm. In these cases, the transverse wavefront distortion of the double-pass amplified beam was less than 0.2 μm for the pump power of 14 kW.

In this study, the slab structure was optimized by considering double-pass amplification for two fixed incident angles. However, the design optimization method of this study can be also applied to other incidence angles. Moreover, it can also predict the wavefront distortion in a much higher power amplification chain using many Nd:YAG slabs. Nevertheless, the wavefront distortion of a real situation may be different from the simulated result. This is because many other factors, such as non-uniformities, can affect the wavefront distortion. However, the simulation method and the results obtained in this study are expected to be helpful in the initial design of a gain medium without any experimental work.

REFERENCES

1. H. Injeyan and G. D. Goodno, *High-power Laser Handbook* (The McGraw-Hill Companies, Inc., China, 2011).
2. G. D. Goodno, S. Palese, J. Harkenrider, and H. Injeyan, "Yb:YAG power oscillator with high brightness and linear polarization," Opt. Lett. **26**, 1672-1674 (2001).
3. G. D. Goodno, H. Komine, S. J. McNaught, S. B. Weiss, S. Redmond, W. Long, R. Simpson, E. C. Cheung, D. Howland, P. Epp, M. Weber, M. McClellan, J. Sollee, and H. Injeyan, "Coherent combination of high-power, zigzag slab lasers," Opt. Lett. **31**, 1247-1249 (2006).
4. G. D. Goodno, C. P. Asman, J. Anderegg, S. Brosnan, E. C. Cheung, D. Hammons, H. Injeyan, H. Komine, W. H. Long, Jr., M. McClellan, S. J. McNaught, S. Redmond, R. Simpson, J. Sollee, M. Weber, S. B. Weiss, and M. Wickham, "Brightness-scaling potential of actively phase-locked solid-state laser arrays," IEEE J. Sel. Topics Quantum Electron. **13**, 460-472 (2007).
5. A. K. Sridharan, S. Saraf, S. Sinha, and R. L. Byer, "Zigzag slabs for solid-state laser amplifiers: batch fabrication and parasitic oscillation suppression," Appl. Opt. **45**, 3340-3351 (2006).
6. W. M. Tulloch, T. S. Rutherford, E. K. Gustafson, and R. L. Byer, "CW high-power conduction-cooled edge-pumped slab laser," Proc. SPIE **3613**, 2-7 (1999).
7. W. M. Tulloch, T. S. Rutherford, E. K. Gustafson, and R. L. Byer, "A 100 W edge-pumped Nd:YAG conduction-cooled slab laser," Adv. Solid-State Lasers **26**, 9-11 (1999).
8. X. Li, H. Xiao, X.-L. Dong, Y.-X. Ma, and X.-J. Xu, "Coherent beam combining of two slab laser amplifier and second-harmonic phase locking based on a multi-dithering technique," Chin. Phys. Lett. **28**, 094210 (2011).
9. S. Li, X. Ma, H. Li, F. Li, X. Zhu, and W. Chen, "Laser-diode-pumped zigzag slab Nd:YAG master oscillator power amplifier," Chin. Phys. Lett. **11**, 071402 (2013).
10. J. S. Shin, Y.-H. Cha, B. H. Cha, H. C. Lee, H. T. Kim, and J. H. Lee, "Simulation of the wavefront distortion and beam quality for a high-power zigzag slab laser," Opt. Commun. **380**, 446-451 (2016).
11. J. S. Shin, Y.-H. Cha, Y. Kim, G. Lim, B. H. Cha, H. C. Lee, S. Kim, and H. T. Kim, "Design of pump beam delivering optical system and doped YAG length to minimize the wavefront distortion in a high-power Nd:YAG zigzag slab laser," Opt. Eng. **56**, 016109 (2017).
12. J. S. Shin, Y.-H. Cha, G. Lim, Y. Kim, S.-O. Kwon, B. H. Cha, H. C. Lee, S. Kim, K. U. Koh, and H. T. Kim, "Wavefront improvement in an end-pumped high power Nd:YAG zigzag slab laser," Opt. Express **25**, 19309-19319 (2017).